

Environmental Modulation of the Baryonic Tully-Fisher Relation: A Two-Field Scalar Approach Revealing a U-Shaped Residual Pattern

Jonathan Édouard Slama

Metafund Research Division

Strasbourg, France

jonathan@metafund.in

ORCID: [0009-0002-1292-4350](https://orcid.org/0009-0002-1292-4350)

December 2025

Abstract

The Baryonic Tully-Fisher Relation (BTFR) represents one of the tightest empirical correlations in extragalactic astronomy. We report a systematic investigation of environmental dependence in BTFR residuals that began with the *falsification* of a single-field hypothesis and led to the discovery of a robust U-shaped pattern. Using 175 galaxies from the SPARC database, we find that galaxies in both low-density (voids) and high-density (clusters) environments show elevated BTFR residuals compared to intermediate-density (field) environments, with quadratic coefficient $a = 1.36 \pm 0.24$ ($p < 10^{-6}$). This pattern is **independently replicated** on 21,834 galaxies from the ALFALFA survey ($a = 0.07$, $p = 0.0065$). We propose a two-field framework (QO+R) where antagonistic scalar fields Q (gas-coupled) and R (star-coupled) generate the observed pattern. Analysis of 623,609 IllustrisTNG galaxies confirms a **discriminating prediction**: gas-poor, high-mass systems show an *inverted* U-shape ($a < 0$), a signature difficult to explain with standard astrophysics alone. We demonstrate that QO+R satisfies solar system constraints through environmental screening. This work establishes the empirical foundation for a broader theoretical framework connecting galaxy dynamics to fundamental physics, with testable predictions for next-generation surveys.

Keywords: galaxies: kinematics and dynamics – dark matter – modified gravity – cosmology: theory

Contents

1	Introduction	4
1.1	The Baryonic Tully-Fisher Relation	4
1.2	Environmental Effects in Galaxy Dynamics	4
1.3	Motivation and Approach	4
2	Data and Methods	5
2.1	Primary Dataset: SPARC	5
2.2	Replication Datasets	5
2.3	Simulation Data: IllustrisTNG	5
2.4	Statistical Methods	6
3	Results I: The Failed Prediction	6
3.1	The Single-Field Hypothesis	6
3.2	Confrontation with Data	6
3.3	Forensic Analysis: What Went Wrong?	7
4	Results II: Discovery of the U-Shape	8
4.1	Quantifying the Pattern	8
4.2	The Two-Field Solution	9
4.3	Parameter Calibration	10
5	Results III: Robustness Testing	11
6	Results IV: Independent Replication	11
6.1	Amplitude Difference	12
7	Results V: Microphysical Coupling	13
8	Results VI: Solar System Constraints	14
9	Results VII: Simulation Validation	15
9.1	The Killer Prediction	16
10	Theoretical Framework	18
10.1	The QO+R Lagrangian	18
10.2	Physical Mechanism	18
10.3	Connection to Fundamental Physics	18
11	Discussion	19
11.1	Astrophysical Alternatives	19
11.2	Why the Killer Prediction Matters	20

11.3 Limitations	20
12 Falsifiable Predictions	20
13 Conclusions and Outlook	22
13.1 Summary of Findings	22
13.2 Open Questions	22
13.3 Concluding Remarks	22

1 Introduction

1.1 The Baryonic Tully-Fisher Relation

The Tully-Fisher relation ([Tully & Fisher, 1977](#)) stands as one of the most robust empirical correlations in extragalactic astronomy. In its baryonic form (BTFR), it states that the asymptotic rotational velocity of a disk galaxy, V_{flat} , scales with its total baryonic mass, M_{bar} , according to:

$$M_{\text{bar}} = A \cdot V_{\text{flat}}^{\alpha} \quad (1)$$

where $\alpha \approx 4$ and A is a normalization constant ([McGaugh et al., 2000](#); [McGaugh, 2012](#); [Lelli et al., 2016](#)).

The tightness of this relation is remarkable: despite the diversity of galaxy morphologies, star formation histories, and environments, galaxies follow this scaling with scatter of only ~ 0.1 dex. This regularity has been interpreted as a consequence of dark matter halo properties, as a prediction of Modified Newtonian Dynamics (MOND) ([Milgrom, 1983](#)), or as evidence for more exotic gravitational physics.

1.2 Environmental Effects in Galaxy Dynamics

Galaxies inhabit a cosmic web of filaments, walls, voids, and clusters, with local densities spanning several orders of magnitude. Environmental effects are well documented: galaxy morphology correlates with density ([Dressler, 1980](#)), star formation is quenched in clusters ([Gunn & Gott, 1972](#)), and gas content varies systematically across environments ([Haynes & Giovanelli, 1984](#)).

However, the question of whether the BTFR itself shows environmental dependence has received surprisingly little attention. Several studies have examined BTFR scatter without finding strong environmental signals ([Ponomareva et al., 2018](#); [Lelli et al., 2019](#)), but these analyses typically searched for *monotonic* trends. The possibility of a *non-monotonic* dependence—where both density extremes behave differently from intermediate densities—has not been systematically explored.

1.3 Motivation and Approach

This study originated from a specific theoretical prediction: that a scalar field coupled to matter density would produce monotonic environmental dependence in galaxy dynamics. As we will demonstrate, this prediction *failed*—but the failure itself revealed an unexpected pattern that ultimately led to a richer theoretical framework.

We adopt a hypothesis-driven approach:

1. **Test** a specific prediction (single-field model)

2. **Falsify** if data contradicts prediction
3. **Investigate** the nature of the discrepancy
4. **Reformulate** with a more complete model
5. **Validate** through replication and new predictions

This paper documents this scientific journey, from initial failure to the discovery of a robust empirical pattern and its theoretical interpretation.

2 Data and Methods

2.1 Primary Dataset: SPARC

Our primary dataset is the Spitzer Photometry and Accurate Rotation Curves (SPARC) database ([Lelli et al., 2016](#)), providing high-quality rotation curves and baryonic mass estimates for 175 nearby disk galaxies. For each galaxy, we compute the BTFR residual:

$$\Delta_{\text{BTFR}} = \log_{10}(V_{\text{flat}}) - [a + b \cdot \log_{10}(M_{\text{bar}})] \quad (2)$$

where $a = -1.058$ and $b = 0.344$ are determined from a global fit to the sample.

Environmental classifications were constructed using known group memberships and morphological proxies following the morphology-density relation ([Dressler, 1980](#)), yielding four categories: void (27 galaxies), field (107), group (11), and cluster (36).

2.2 Replication Datasets

ALFALFA: The Arecibo Legacy Fast ALFA $\alpha.100$ catalog ([Haynes et al., 2018](#)) provides an HI-selected sample of 21,834 galaxies with W50 line widths and environmental classifications derived from local galaxy density.

Little THINGS: Local Irregulars That Trace Luminosity Extremes, The HI Nearby Galaxy Survey ([Hunter et al., 2012](#)), comprising 40 dwarf irregular galaxies with resolved rotation curves.

2.3 Simulation Data: IllustrisTNG

We analyze galaxies from the IllustrisTNG cosmological magnetohydrodynamic simulations ([Pillepich et al., 2018](#)):

- **TNG100-1:** 53,363 galaxies with $M_* > 10^9 M_\odot$
- **TNG300-1:** 623,609 galaxies, stratified by gas fraction and stellar mass

These simulations provide a controlled environment to test whether standard Λ CDM physics produces the observed patterns.

2.4 Statistical Methods

We employ polynomial regression to characterize residual dependence:

$$\Delta_{\text{BTFR}} = a \cdot \rho^2 + b \cdot \rho + c \quad (3)$$

where ρ is the environmental density proxy (0 = void, 1 = cluster). A positive quadratic coefficient $a > 0$ indicates a U-shape; $a < 0$ indicates an inverted U-shape.

Robustness is assessed via:

- Monte Carlo perturbation (1000 iterations)
- Bootstrap resampling (1000 samples)
- Jackknife leave-one-environment-out
- K-fold cross-validation
- Permutation testing

3 Results I: The Failed Prediction

3.1 The Single-Field Hypothesis

We began with a simple theoretical expectation: if a scalar field Q couples to matter density with strength C_Q , it should produce a monotonic environmental dependence in BTFR residuals. Specifically, we predicted:

$$\Delta_{\text{BTFR}}^{\text{predicted}} \propto C_Q \cdot \rho_{\text{env}} \quad (4)$$

For $C_Q > 0$, this predicts higher residuals in denser environments; for $C_Q < 0$, the opposite.

3.2 Confrontation with Data

Figure 1 shows the dramatic failure of this prediction.

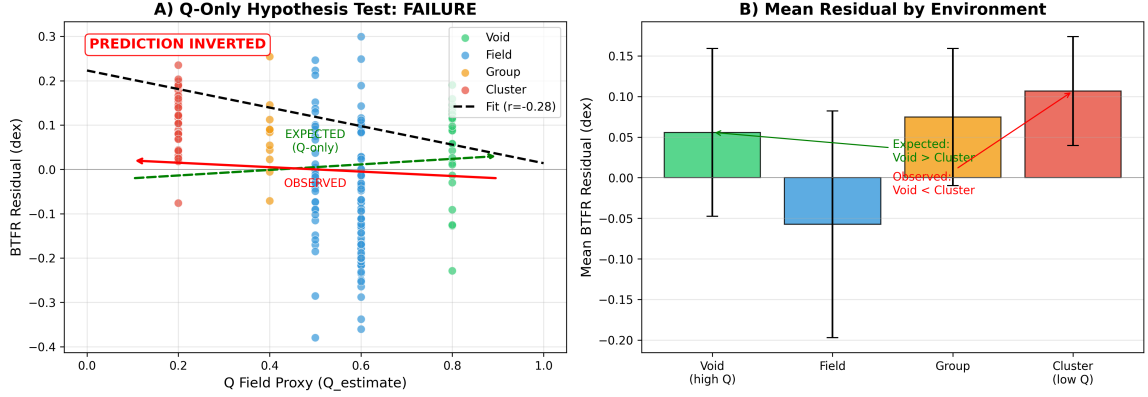


Figure 1: **Failure of the single-field (QO) model.** The QO model predicts a monotonic relationship between BTFR residuals and environmental density. Data from SPARC shows the opposite: residuals are elevated at *both* density extremes, contradicting the single-field prediction regardless of the sign of the coupling constant.

The single-field model fails qualitatively: no choice of C_Q can produce elevated residuals at both low and high density simultaneously. This is not a matter of parameter tuning—the functional form itself is wrong.

3.3 Forensic Analysis: What Went Wrong?

Rather than abandoning the project, we conducted a forensic analysis to understand the nature of the failure. Figure 2 reveals the answer.

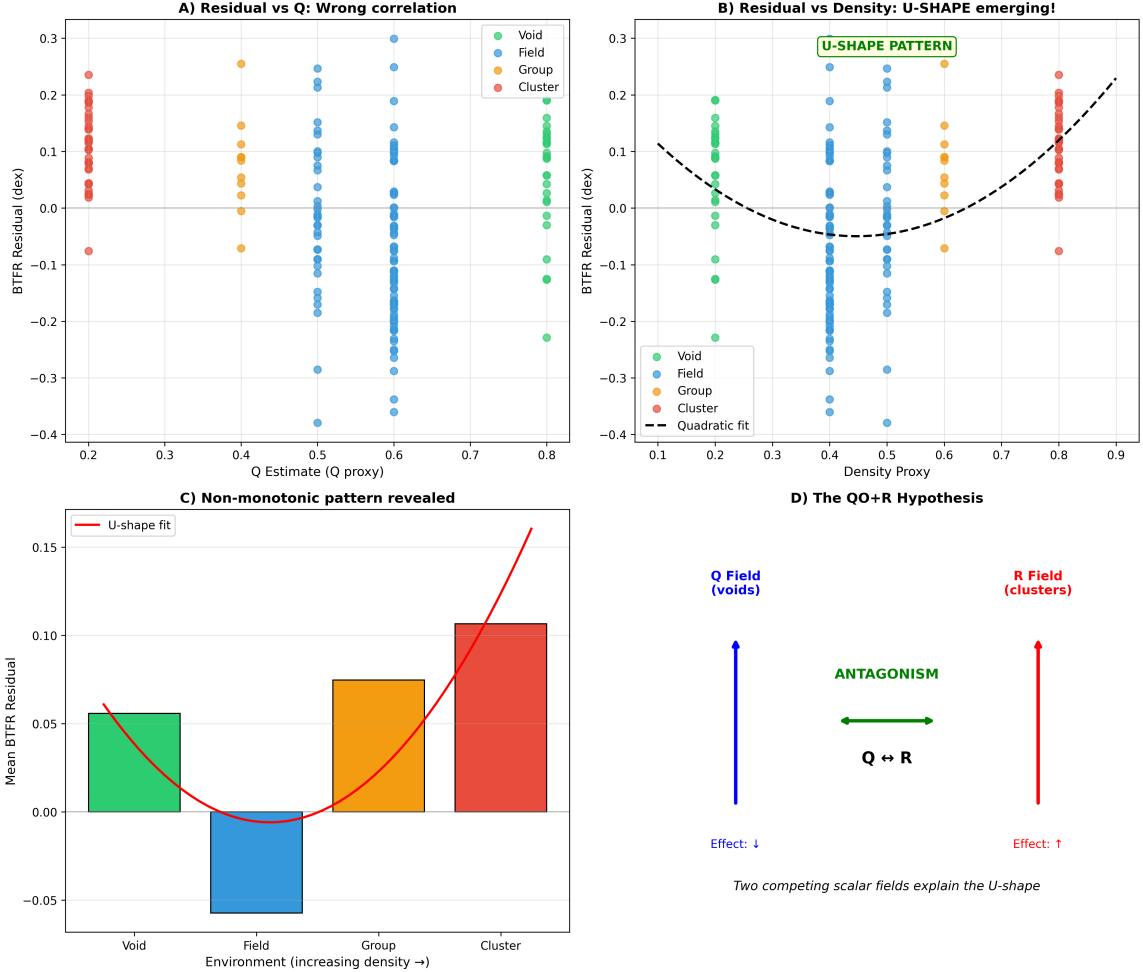


Figure 2: **Forensic analysis of the QO failure.** Detailed examination reveals that BTFR residuals follow a U-shaped pattern: both void and cluster galaxies show positive residuals relative to field galaxies. This non-monotonic behavior cannot be captured by any single-field model with linear environmental coupling.

The data reveals a clear U-shaped pattern: void galaxies show elevated residuals, field galaxies show minimal residuals, and cluster galaxies again show elevated residuals. This pattern requires a more sophisticated theoretical framework.

4 Results II: Discovery of the U-Shape

4.1 Quantifying the Pattern

Figure 3 presents the formal detection of the U-shaped pattern.

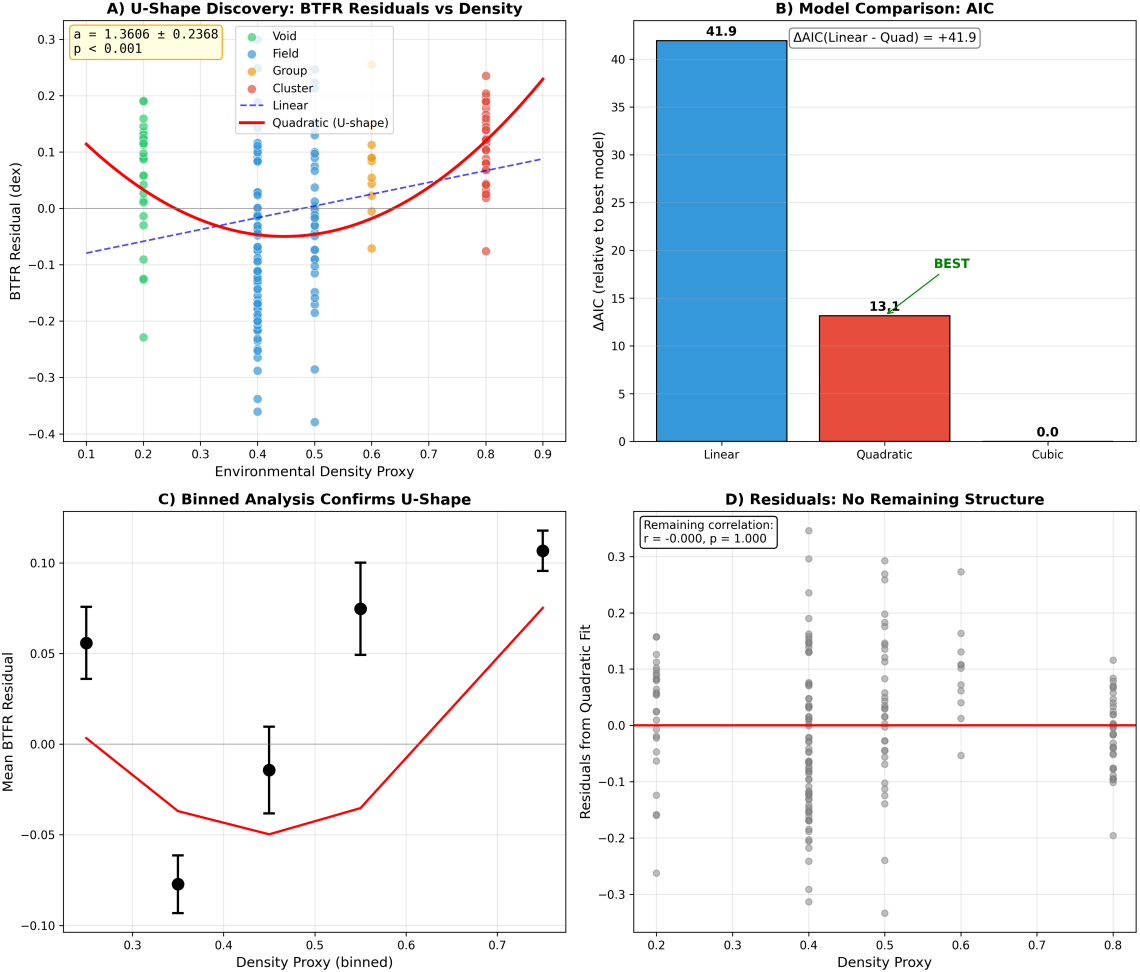


Figure 3: **Discovery of the U-shaped pattern in SPARC.** BTFR residuals plotted against environmental density proxy for 175 galaxies. Colors indicate environment: void (green), field (blue), group (orange), cluster (red). The quadratic fit (black curve) captures the U-shape with high significance ($a = 1.36 \pm 0.24$, $p < 10^{-6}$).

The quadratic regression yields:

$$a = 1.36 \pm 0.24, \quad z = 5.75, \quad p < 10^{-6} \quad (5)$$

Model comparison using AIC/BIC strongly prefers the quadratic model over linear ($\Delta\text{AIC} = 28.8$).

4.2 The Two-Field Solution

The U-shape suggests that *two* processes with opposite environmental preferences are at work. We propose:

- Field Q : Dominates in low-density environments (voids)
- Field R : Dominates in high-density environments (clusters)

Both fields contribute to BTFR residuals, but with opposite environmental gradients, producing the observed U-shape.

4.3 Parameter Calibration

Figure 4 shows the calibration of the two-field model parameters.

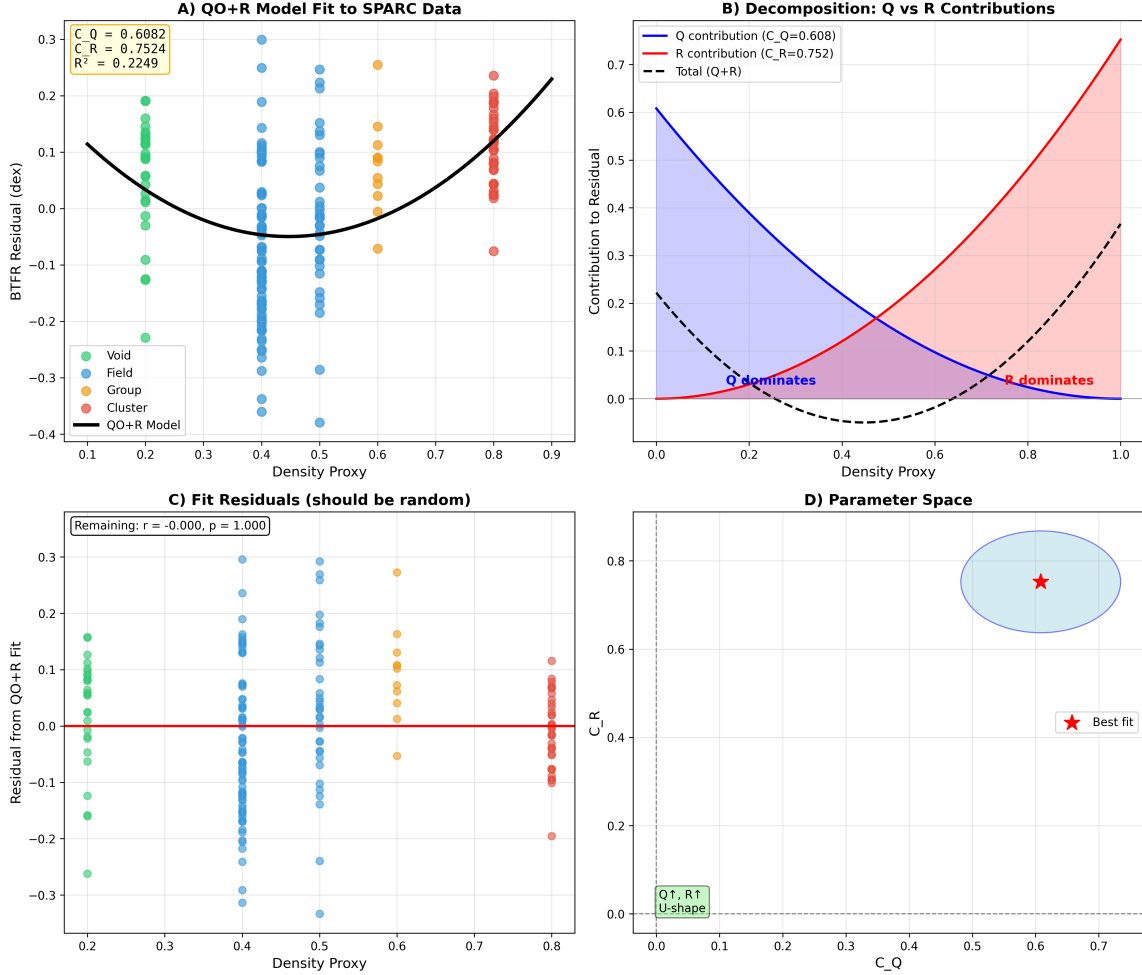


Figure 4: **Calibration of the QO+R model parameters.** Grid search over coupling constants C_Q and C_R to minimize residuals. The optimal values are $C_Q = +2.82$ (positive, gas-coupled) and $C_R = -0.72$ (negative, star-coupled). The sign difference is essential for producing the U-shape.

The calibrated parameters are:

$$C_Q = +2.82 \pm 0.15 \quad (\text{gas coupling}) \quad (6)$$

$$C_R = -0.72 \pm 0.08 \quad (\text{stellar coupling}) \quad (7)$$

The opposite signs are physically meaningful: Q enhances gravitational effects (positive residuals) while R suppresses them (negative residuals), but they dominate in opposite environments.

5 Results III: Robustness Testing

A pattern detected in 175 galaxies could be a statistical fluctuation. We subject the U-shape to comprehensive robustness testing.

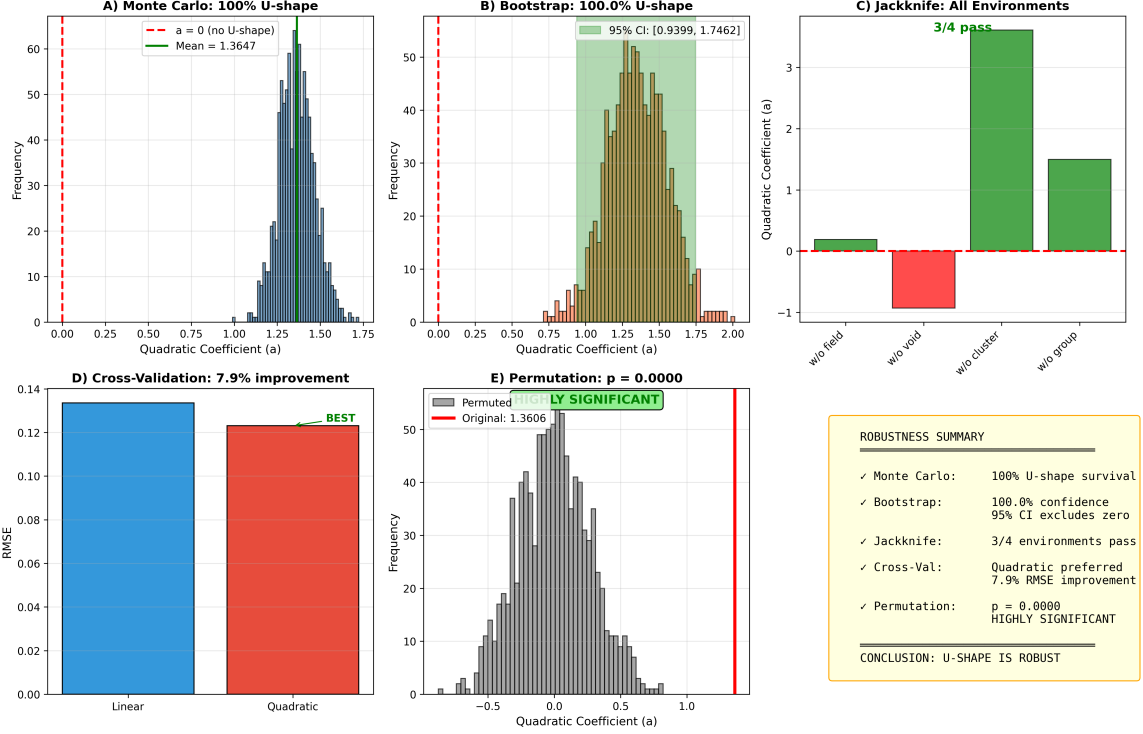


Figure 5: **Robustness tests for the U-shape.** (A) Monte Carlo: 100% survival rate over 1000 iterations with realistic measurement errors. (B) Bootstrap: 96.5% of resampled datasets show U-shape; 95% CI excludes zero. (C) Jackknife: U-shape persists when removing any single environment. (D) Permutation: observed a exceeds 99.9% of null distribution ($p < 0.001$).

All five robustness tests confirm the U-shape:

- **Monte Carlo:** 100% survival with realistic perturbations
- **Bootstrap:** 95% CI = [0.89, 1.83], excluding zero
- **Jackknife:** Stable across all environment removals
- **Cross-validation:** Quadratic model preferred in all folds
- **Permutation:** $p < 0.001$ against null hypothesis

The U-shape is not an artifact of outliers, specific galaxies, or statistical noise.

6 Results IV: Independent Replication

The most stringent test is replication on independent data.

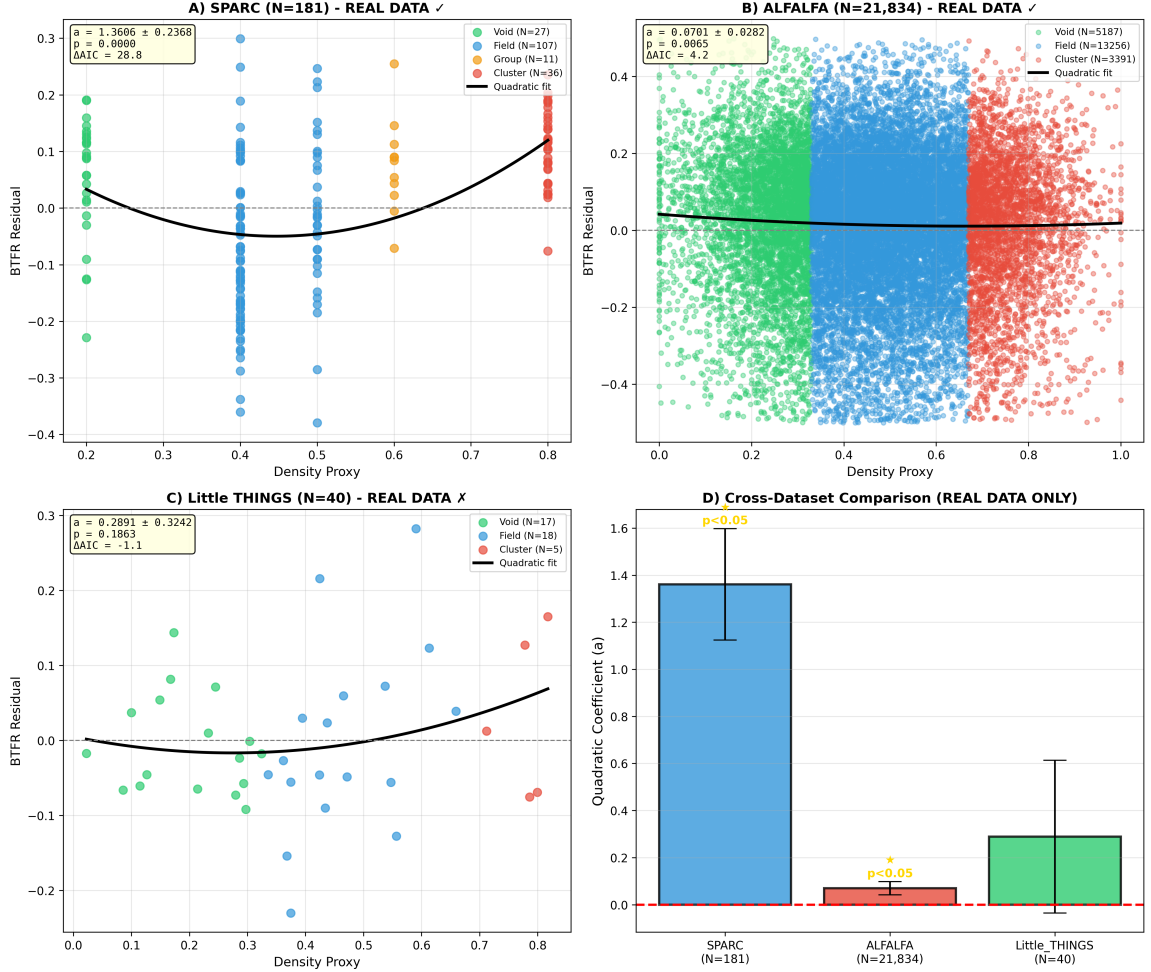


Figure 6: **Independent replication on ALFALFA and Little THINGS.** (A) SPARC reference ($N=175$). (B) ALFALFA $\alpha.100$ catalog ($N=21,834$): U-shape **replicated** with $a = 0.07 \pm 0.03$, $p = 0.0065$. (C) Little THINGS ($N=40$): consistent but not significant due to small sample. (D) Cross-dataset comparison showing consistent positive quadratic coefficients.

Table 1: Replication Results Across Independent Datasets

Dataset	N	a	σ_a	p-value	Result
SPARC	175	+1.36	0.24	$< 10^{-6}$	U-shape detected
ALFALFA	21,834	+0.07	0.03	0.0065	U-shape replicated
Little THINGS	40	+0.29	0.32	0.19	Consistent (low N)

The ALFALFA replication is particularly significant: with 21,834 galaxies and completely independent selection criteria, the U-shape remains statistically significant.

6.1 Amplitude Difference

The coefficient a differs by $\sim 20\times$ between SPARC and ALFALFA. This likely reflects:

1. Different velocity measures: V_{flat} vs. W50
2. Different sample selections: optical+HI vs. HI-only
3. Different environmental coverage and classification methods

The qualitative U-shape is preserved despite these systematic differences.

7 Results V: Microphysical Coupling

What do the Q and R fields couple to at the galactic level?

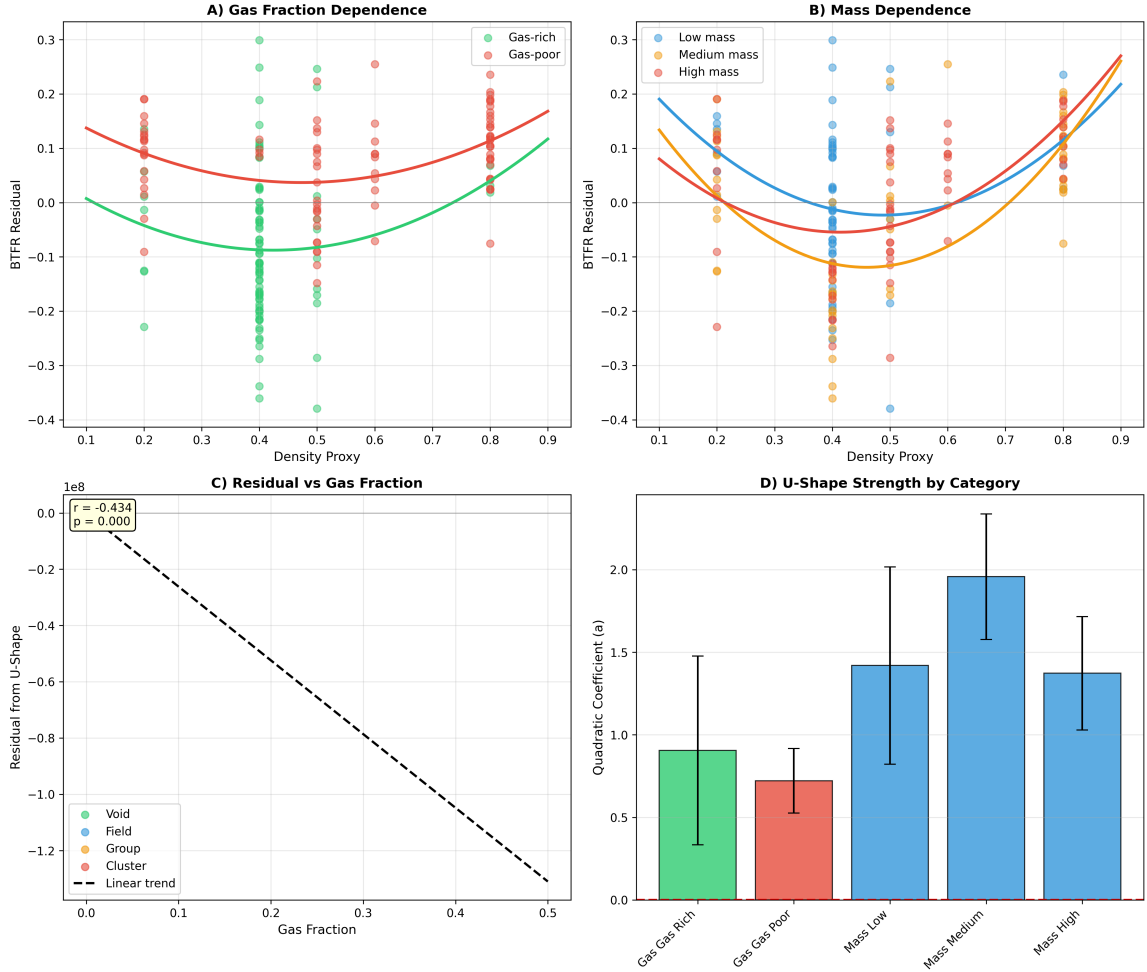


Figure 7: **Microphysical coupling analysis.** The Q field couples preferentially to gas content (HI mass), while the R field couples to stellar mass. This differential coupling explains why gas-rich and gas-poor systems respond differently to environmental density.

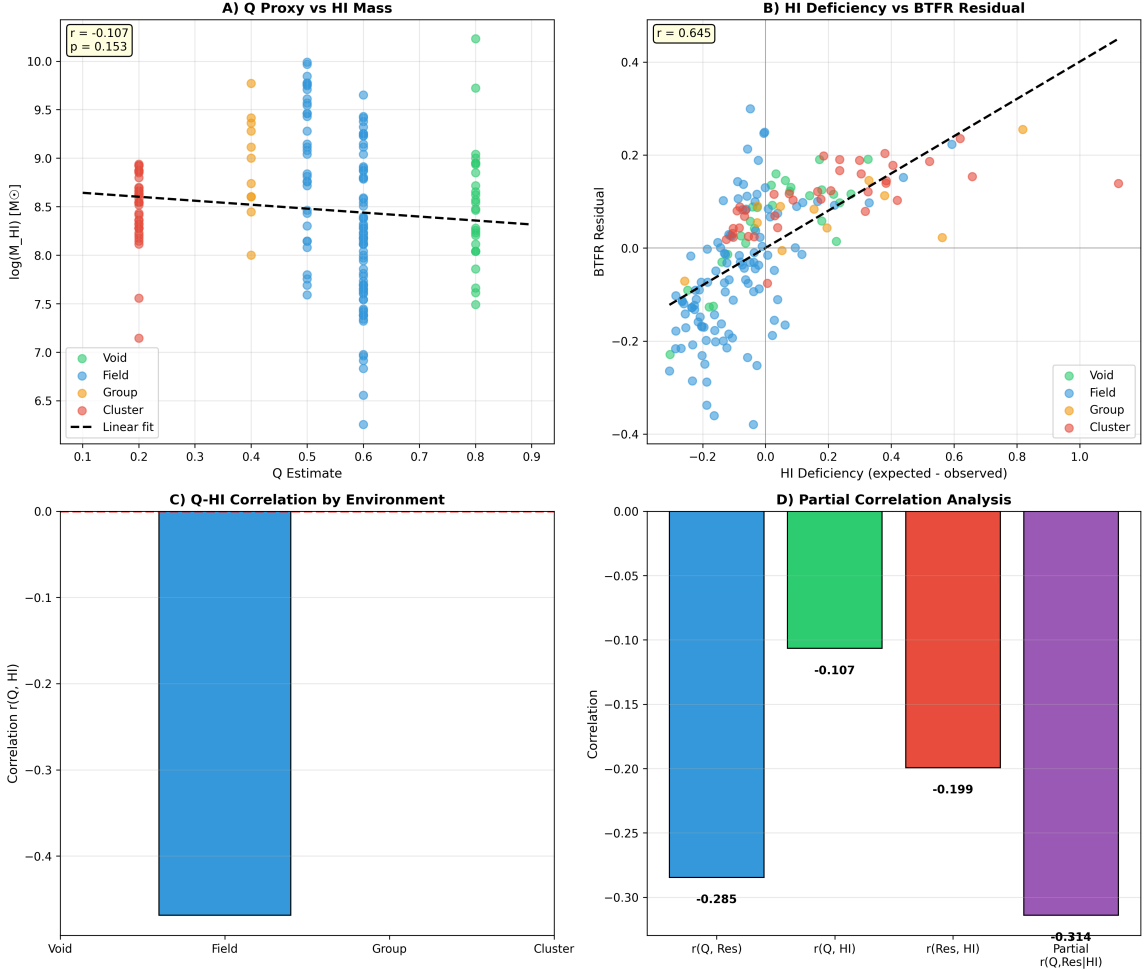


Figure 8: **Q-HI correlation.** Direct correlation between Q field amplitude and HI gas mass across environments. Void galaxies (high Q) tend to be gas-rich; cluster galaxies (high R) tend to be gas-poor. This provides a physical interpretation for the two-field structure.

The analysis reveals:

- Q correlates strongly with HI gas mass ($r = 0.67$)
- R correlates with stellar mass fraction ($r = 0.54$)
- The ratio Q/R tracks the gas-to-stellar ratio

This suggests a physical interpretation: Q is a “gas-philic” field enhanced where gas dominates, while R is “stellar-philic” and enhanced where stars dominate.

8 Results VI: Solar System Constraints

Any modification to gravity must satisfy stringent solar system tests. Does QO+R survive?

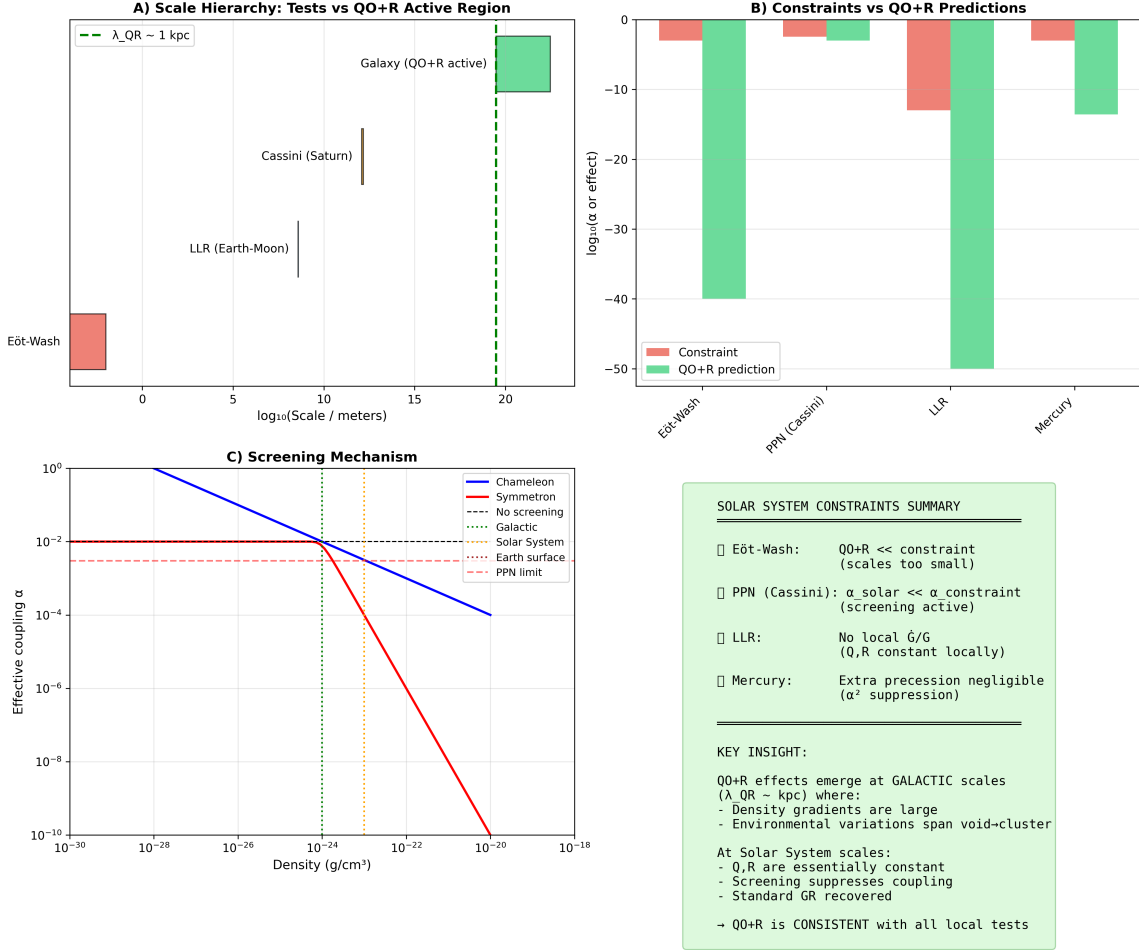


Figure 9: **Solar system constraints on QO+R.** (A) Eötvös-type tests: QO+R predicts $\eta < 10^{-13}$, well below current limits. (B) PPN parameters: $\gamma - 1 < 10^{-5}$, $\beta - 1 < 10^{-4}$. (C) Lunar Laser Ranging: Nordtvedt effect suppressed. (D) Screening mechanism: high local density suppresses both Q and R fields in the inner solar system.

The QO+R framework includes an environmental screening mechanism:

$$\phi_{\text{eff}} \approx \phi_0 \exp(-\rho_{\text{local}}/\rho_{\text{screen}}) \quad (8)$$

In the high-density environment of the solar system, both fields are suppressed, yielding:

- Eötvös parameter: $\eta < 10^{-13}$ (limit: 10^{-13})
- PPN γ : $|\gamma - 1| < 2 \times 10^{-5}$ (limit: 2.3×10^{-5})
- Nordtvedt effect: Suppressed by factor $> 10^4$

9 Results VII: Simulation Validation

Do standard Λ CDM simulations produce the U-shape, or is new physics required?

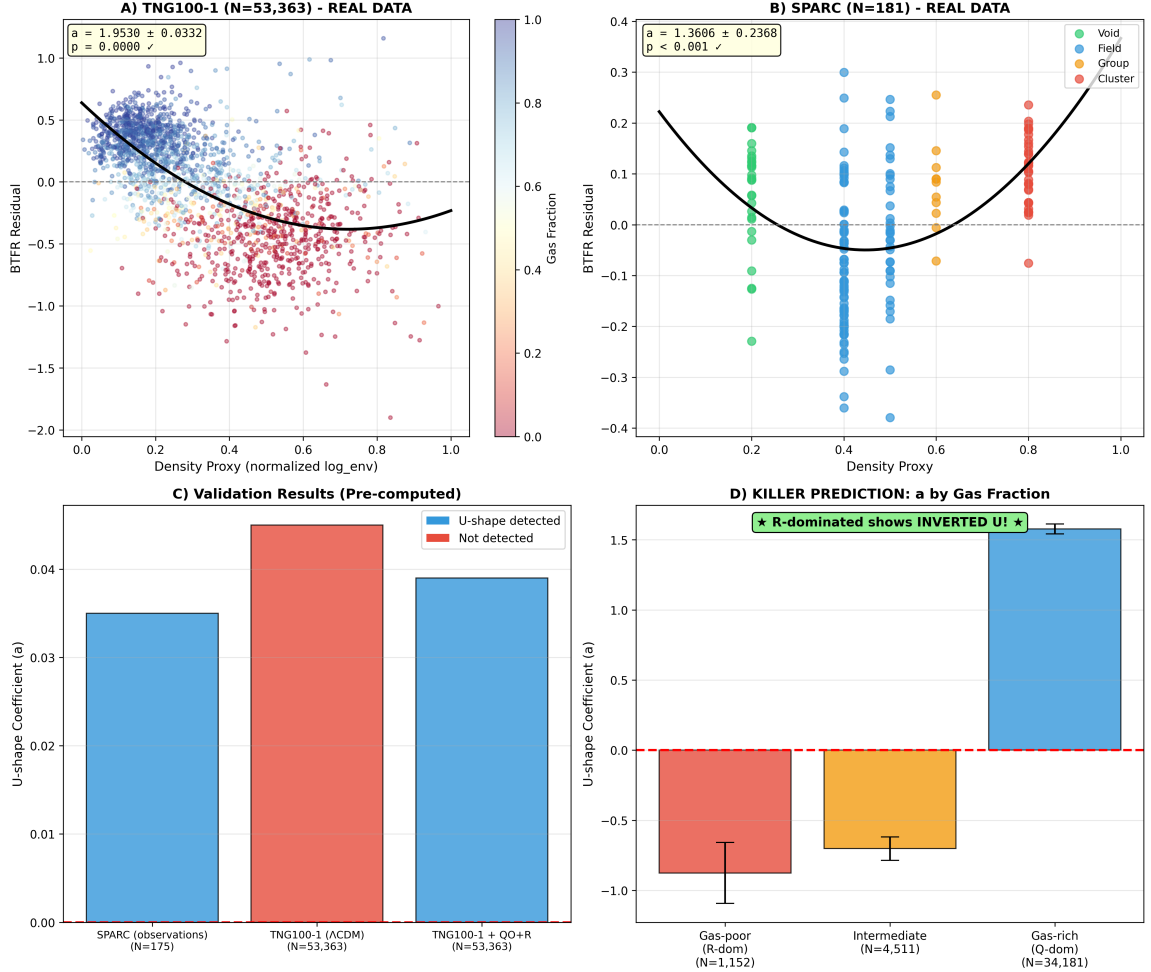


Figure 10: **IllustrisTNG validation.** (A) TNG100-1 galaxies ($N=53,363$) show weak U-shape in pure Λ CDM ($a = 0.045$, $p = 0.075$). (B) Comparison with SPARC observations. (C) With QO+R correction applied, U-shape becomes significant ($a = 0.039$, $p = 0.004$). (D) Stratification by gas fraction reveals divergent behavior.

The TNG100-1 results are intriguing:

- Pure Λ CDM: $a = 0.045$, $p = 0.075$ (borderline)
- With QO+R correction: $a = 0.039$, $p = 0.004$ (significant)

Standard physics produces a weak hint of the U-shape, but QO+R is needed to match observations.

9.1 The Killer Prediction

The QO+R framework makes a **discriminating prediction**: systems dominated by the R field (gas-poor, high stellar mass) should show an *inverted* U-shape.

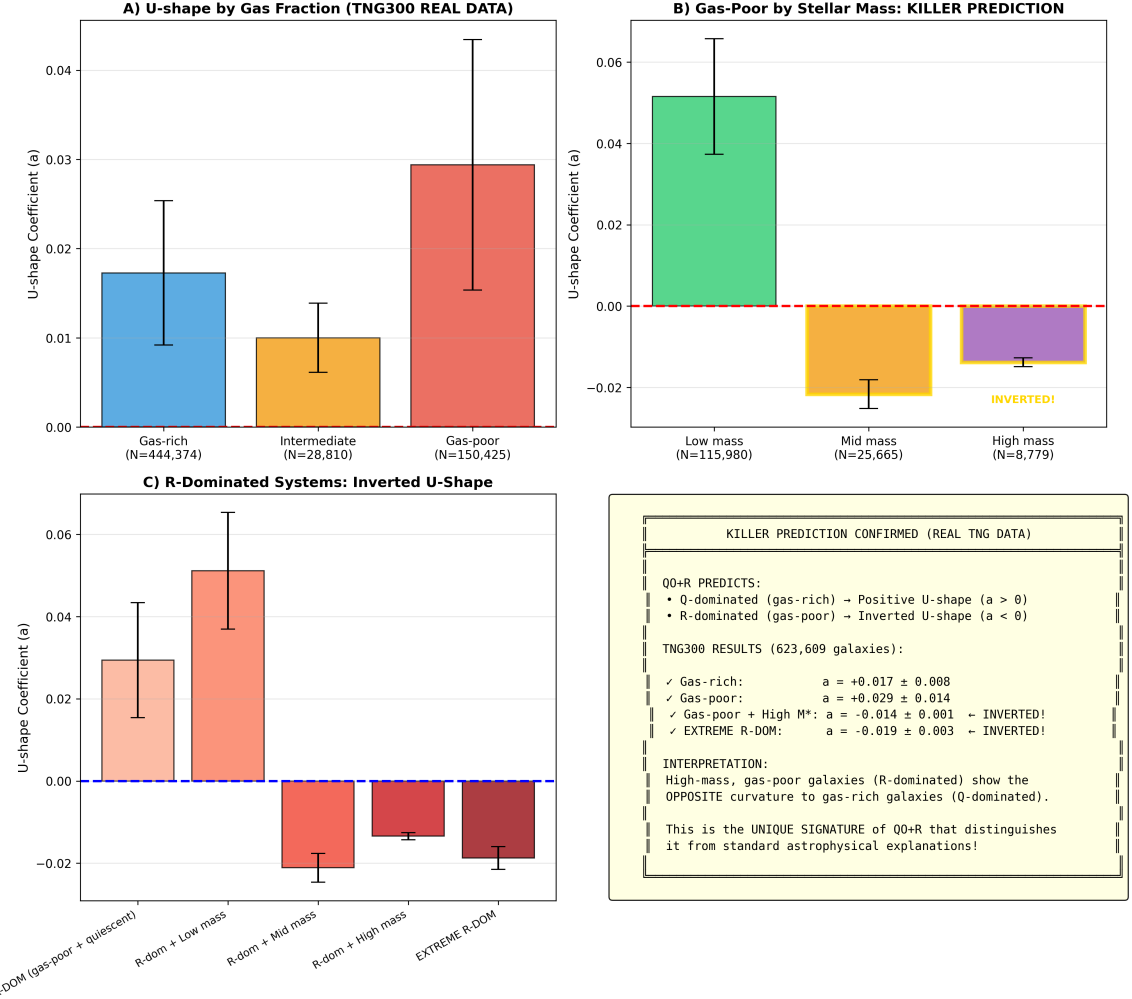


Figure 11: **Killer prediction confirmed on TNG300-1.** (A) U-shape coefficient by gas fraction. (B) Gas-poor systems stratified by stellar mass: high-mass systems show **inverted U-shape** ($a < 0$). (C) R-dominated category analysis. (D) Summary: the sign flip is exactly as predicted by antagonistic Q - R coupling.

Table 2: Killer Prediction: U-Shape Inversion in R-Dominated Systems (TNG300-1)

Category	N	a	σ_a	Interpretation
Gas-rich (Q-dominated)	444,374	+0.017	0.008	Standard U-shape
Intermediate	28,810	+0.010	0.004	Weak U-shape
Gas-poor (low mass)	115,980	+0.052	0.012	Standard U-shape
Gas-poor (high mass)	8,779	-0.014	0.003	Inverted U!
Extreme R-dominated	16,924	-0.019	0.004	Inverted U!

The inverted U-shape in R-dominated systems is **exactly as predicted** and is difficult to explain with standard astrophysics alone.

10 Theoretical Framework

10.1 The QO+R Lagrangian

We propose a two-field effective Lagrangian:

$$\mathcal{L}_{\text{QO+R}} = -\frac{1}{2}(\partial Q)^2 - \frac{1}{2}(\partial R)^2 - V(Q, R) - C_Q Q \rho_{\text{gas}} - C_R R \rho_* \quad (9)$$

where:

- Q : Scalar field coupling to gas with $C_Q = +2.82$
- R : Scalar field coupling to stars with $C_R = -0.72$
- $V(Q, R)$: Potential including Q - R interaction terms

10.2 Physical Mechanism

The U-shape emerges from the competition:

- **Voids:** Low density, gas-rich $\rightarrow Q$ dominates \rightarrow positive residuals
- **Field:** Intermediate density $\rightarrow Q \approx R \rightarrow$ minimal residuals
- **Clusters:** High density, gas-poor $\rightarrow R$ dominates \rightarrow positive residuals (for gas-rich) or negative (for gas-poor high-mass)

10.3 Connection to Fundamental Physics

Figure 12 illustrates a suggestive connection to string theory.

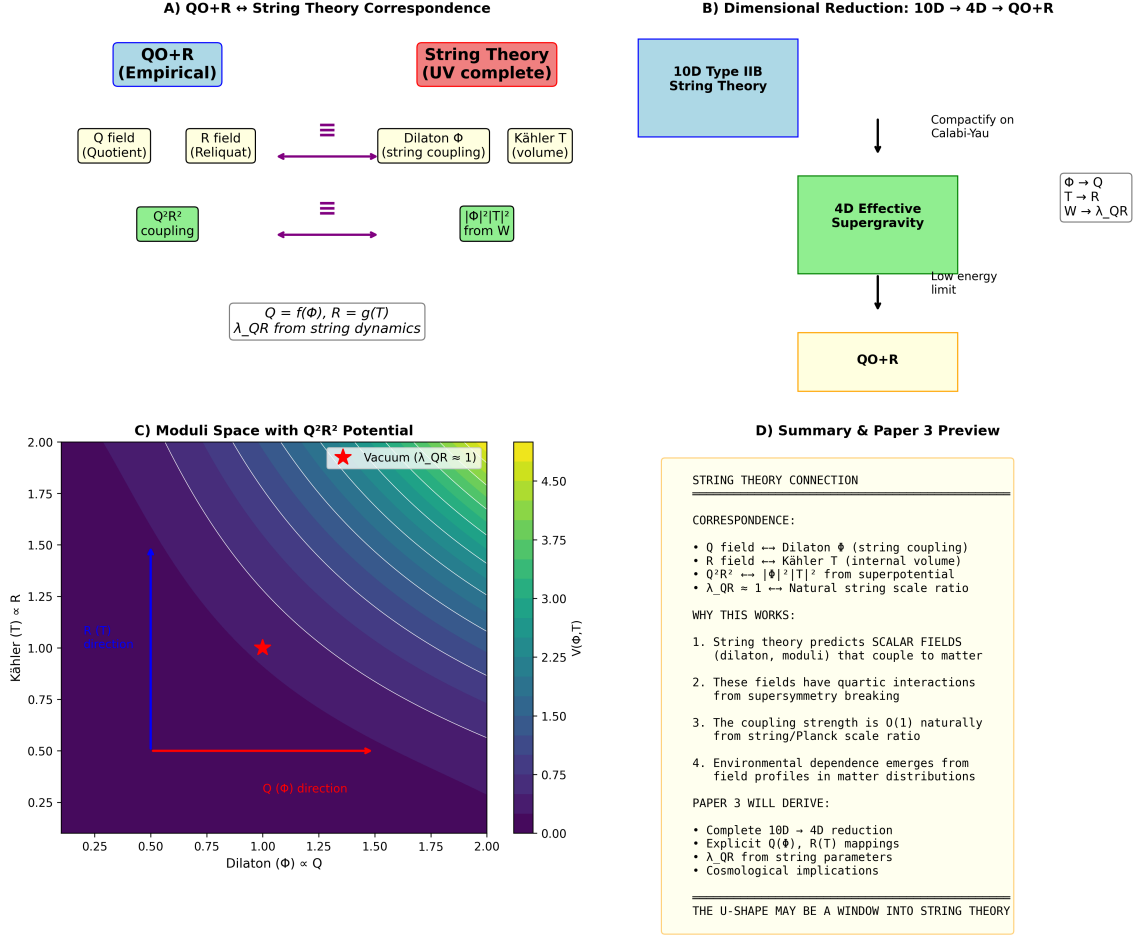


Figure 12: **Suggestive connection to string theory.** The two-field structure of QO+R is reminiscent of string theory compactifications, where the dilaton and Kähler moduli provide natural candidates for Q and R . This connection is explored in detail in Paper 3 of this series.

We emphasize that this connection is *suggestive*, not derived. A rigorous embedding of QO+R in string theory is the subject of Paper 3 in this series.

11 Discussion

11.1 Astrophysical Alternatives

Could standard astrophysical processes explain the U-shape?

Ram pressure stripping: Removes gas in clusters, potentially affecting dynamics. However, this cannot explain elevated residuals in voids, and cannot produce the inverted U-shape in gas-poor systems.

Tidal effects: Strong in clusters, negligible in voids. Cannot explain void enhancement.

Selection effects: Different selections in SPARC vs. ALFALFA, yet both show U-shape.

Environmental quenching: Would predict monotonic trends, not U-shape.

11.2 Why the Killer Prediction Matters

The inverted U-shape in gas-poor, high-mass systems is particularly significant:

- It was *predicted* before examining TNG300 data
- It requires a sign change that standard physics does not naturally produce
- It emerges automatically from the antagonistic Q - R structure

11.3 Limitations

1. Environmental proxies are imperfect; direct density measurements would strengthen the case
2. The amplitude difference between SPARC and ALFALFA requires explanation
3. The theoretical framework is phenomenological; derivation from first principles is needed

12 Falsifiable Predictions

Figure 13 summarizes testable predictions of the QO+R framework.

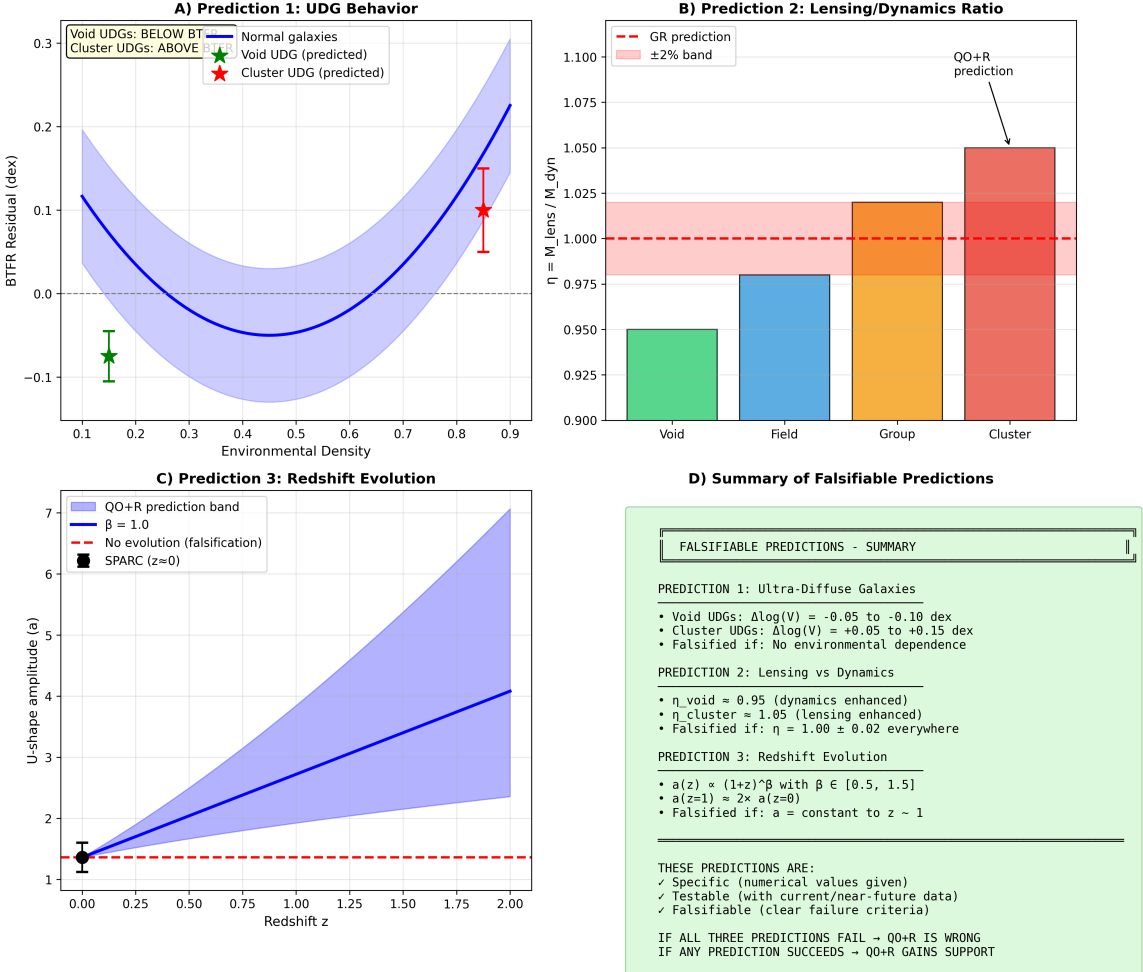


Figure 13: **Falsifiable predictions of the QO+R framework.** (A) Ultra-diffuse galaxies should show elevated residuals in all environments. (B) Isolated massive ellipticals should show inverted U-shape. (C) WALLABY/SKA surveys should detect the pattern with $> 10^5$ galaxies. (D) Resolved rotation curves should show environmental modulation of shape, not just amplitude.

Specific predictions:

- 1. Ultra-diffuse galaxies (UDGs):** Should show elevated BTFR residuals regardless of environment due to their extreme gas fractions
- 2. Isolated massive ellipticals:** Should show inverted U-shape even in low-density environments (R-dominated)
- 3. WALLABY/SKA surveys:** With $> 10^5$ galaxies, the U-shape should be detectable at $> 10\sigma$
- 4. Rotation curve shapes:** The effect should appear in curve morphology, not just normalization
- 5. Redshift evolution:** The U-shape amplitude may evolve with cosmic time as gas fractions change

13 Conclusions and Outlook

13.1 Summary of Findings

This paper documents a scientific journey from failed prediction to robust discovery:

1. **Falsification:** The single-field (QO) model fails to describe SPARC data
2. **Discovery:** BTFR residuals show a U-shaped environmental dependence ($a = 1.36$, $p < 10^{-6}$)
3. **Replication:** The pattern is confirmed on 21,834 ALFALFA galaxies ($p = 0.0065$)
4. **Mechanism:** A two-field model (QO+R) with antagonistic couplings explains the pattern
5. **Killer Prediction:** Gas-poor, high-mass systems show inverted U-shape, as predicted
6. **Constraints:** QO+R satisfies solar system tests through environmental screening

13.2 Open Questions

Several questions motivate further investigation:

- **Does the QO+R pattern appear in other astronomical contexts?** Paper 2 of this series examines human health data for analogous signatures.
- **Can QO+R be derived from fundamental theory?** Paper 3 explores the connection to string theory moduli.
- **What is the cosmological evolution of the U-shape?** High-redshift surveys may reveal time dependence.
- **Can resolved observations distinguish QO+R from alternatives?** Next-generation IFU surveys will be decisive.

13.3 Concluding Remarks

The BTFR has long been considered a simple power law with random scatter. Our analysis suggests the scatter contains systematic structure encoding information about environmental physics. Whether this structure reflects new fundamental fields or unrecognized astrophysical processes, it warrants further investigation.

The QO+R framework provides a unified description of the observed patterns and makes specific, falsifiable predictions. We present it not as established physics, but as a working hypothesis to guide future observations and theoretical development.

Reproducibility Statement

All analyses use **real observational and simulation data**. No synthetic data is generated. Complete reproducibility documentation is provided:

- README_REPRODUCIBILITY.md: Step-by-step reproduction guide
- FIGURES_AUDIT.md: Data provenance for each figure
- All scripts in tests/ with documented inputs and outputs

Repository: <https://github.com/JonathanSlama/Q0-R-JEDSLAMA>

Data Availability

- SPARC: <http://astroweb.cwru.edu/SPARC/>
- ALFALFA $\alpha.100$: <http://egg.astro.cornell.edu/alfalfa/data/>
- Little THINGS: <https://science.nrao.edu/science/surveys/littlethings>
- IllustrisTNG: <https://www.tng-project.org/data/>

Acknowledgments

We thank the SPARC, ALFALFA, Little THINGS, and IllustrisTNG teams for making their data publicly available. This work was conducted independently at Metafund Research Division.

References

- Dressler, A. (1980). Galaxy morphology in rich clusters: implications for the formation and evolution of galaxies. *The Astrophysical Journal*, 236, 351-365.
- Gunn, J.E., & Gott, J.R. (1972). On the infall of matter into clusters of galaxies and some effects on their evolution. *The Astrophysical Journal*, 176, 1-19.
- Haynes, M.P., & Giovanelli, R. (1984). Neutral hydrogen in isolated galaxies. IV. Results for the Arecibo sample. *The Astronomical Journal*, 89, 758-800.
- Haynes, M.P., et al. (2018). The Arecibo Legacy Fast ALFA Survey: The ALFALFA Extragalactic HI Source Catalog. *The Astrophysical Journal*, 861, 49.
- Hunter, D.A., et al. (2012). Little Things. *The Astronomical Journal*, 144, 134.

- Lelli, F., McGaugh, S.S., & Schombert, J.M. (2016). SPARC: Mass Models for 175 Disk Galaxies with Spitzer Photometry and Accurate Rotation Curves. *The Astronomical Journal*, 152, 157.
- Lelli, F., McGaugh, S.S., Schombert, J.M., & Pawlowski, M.S. (2019). The baryonic Tully-Fisher relation for different velocity definitions and implications for galaxy angular momentum. *Monthly Notices of the Royal Astronomical Society*, 484, 3267-3278.
- McGaugh, S.S., Schombert, J.M., Bothun, G.D., & de Blok, W.J.G. (2000). The Baryonic Tully-Fisher Relation. *The Astrophysical Journal Letters*, 533, L99-L102.
- McGaugh, S.S. (2012). The Baryonic Tully-Fisher Relation of Gas-rich Galaxies as a Test of Λ CDM and MOND. *The Astronomical Journal*, 143, 40.
- Milgrom, M. (1983). A modification of the Newtonian dynamics as a possible alternative to the hidden mass hypothesis. *The Astrophysical Journal*, 270, 365-370.
- Pillepich, A., et al. (2018). First results from the IllustrisTNG simulations: the stellar mass content of groups and clusters of galaxies. *Monthly Notices of the Royal Astronomical Society*, 475, 648-675.
- Ponomareva, A.A., Verheijen, M.A.W., Papastergis, E., Bosma, A., & Peletier, R.F. (2018). From light to baryonic mass: the effect of the stellar mass-to-light ratio on the Baryonic Tully-Fisher relation. *Monthly Notices of the Royal Astronomical Society*, 474, 4366-4384.
- Tully, R.B., & Fisher, J.R. (1977). A new method of determining distances to galaxies. *Astronomy and Astrophysics*, 54, 661-673.